

Enhanced Rashba spin-orbit coupling in core-shell nanowires by the interfacial effect

Paweł Wójcik,^{1, a)} Andrea Bertoni,^{2, b)} and Guido Goldoni^{3, 2, c)}

¹⁾ AGH University of Science and Technology, Faculty of Physics and Applied Computer Science, 30-059 Krakow, Al. Mickiewicza 30, Poland

²⁾ S3, Istituto Nanoscienze-CNR, Via Campi 213/a, 41125 Modena, Italy

³⁾ Department of Physics, Informatics and Mathematics, University of Modena and Reggio Emilia, Italy

(Dated: November 26, 2018)

We report on $\vec{k} \cdot \vec{p}$ calculations of Rashba spin-orbit coupling controlled by external gates in InAs/InAsP core-shell nanowires. We show that charge spilling in the barrier material allows for a stronger symmetry breaking than in homogeneous nano-materials, inducing a specific interface-related contribution to spin-orbit coupling. Our results qualitatively agree with recent experiments [S. Futhemeier *et al.*, Nat. Commun. **7**, 12413 (2016)] and suggest additional wavefunction engineering strategies to enhance and control spin-orbit coupling.

Understanding and controlling spin-orbit coupling (SOC) is critical in semiconductor physics. In particular, in semiconductor nanowires (NWs)^{1–7} SOC is essential for the development of a suitable hardware for topological quantum computation^{8,9}, with qubits encoded in zero-mode Majorana states which are supported by hybrid semiconductor-superconductor NWs^{10–15}. Among other parameters, qubit protection at sufficiently high temperatures relies on a large SOC which determines the topological gap. Additionally, electrical control of SOC is necessary in the realization of spintronic devices^{16–26}.

SOC arises from the absence of inversion symmetry of the electrostatic potential. In semiconductor NWs, typically having a prismatic shape, finite SOC may be induced by distorting the quantum confinement (Rashba SOC²⁷) by means of external gates, with the advantage of electrical control. A lattice contribution (Dresselhaus SOC²⁸) is typically small and may vanish in specific crystallographic directions - for zincblende NWs, the Dresselhaus term vanishes along [111] due to the inversion symmetry.

The Rashba SOC constant α_R has been investigated experimentally in homogeneous NWs based on the strong SOC materials InSb^{29,30} and InAs^{31–35}. Recently⁵, we reported on a $\vec{k} \cdot \vec{p}$ approach applied to *homogeneous* NWs which predicts α_R from compositional and structural parameters only. Our calculations performed for InSb NWs⁵ and InAs NWs³⁶ generally confirm recent experiments in homogeneous NWs^{29,31}, exposing values of α_R exceeding by one order of magnitude those reported for 2D analogous planar systems^{37–39}. Moreover, α_R proved to be strongly tunable with external gates in samples and configurations which can be routinely realized with current technology.

For a quantitative prediction of SOC, it is necessary to take into account valence-to-conduction band coupling, the explicit geometry and crystal structure of the NW, and the electron gas distribution which, in turn, must be self-consistently determined by quantum confinement effects, interaction with dopants and electron-electron interaction. Indeed, in NWs the electron gas localization, and ensuing SOC, is a non-trivial result of competing energy contributions. As a function of doping concentration and ensuing free charge density, the electron gas evolves from a broad cylindrical distribution in the NW core (low density regime) to coupled quasi-1D and quasi-2D channels at the NW edges (large density regime)^{40–43}. Until polygonal symmetry holds, $\alpha_R = 0$ regardless. However, external gates easily remove the symmetry; again, how α_R moves from zero under the influence of the external gates strongly depends on the charge density regime⁵.

In this Letter we extend and apply the $\vec{k} \cdot \vec{p}$ approach to core-shell NWs (CSNWs) and expose a novel mechanism through which SOC can be further tailored, and possibly enhanced. Epitaxially overgrown shells are often used in NW technology, either as a passivating layer improving optical performance⁴⁴, or as a technique to engineer radial heterostructures⁴⁵. Here we show that CSNWs

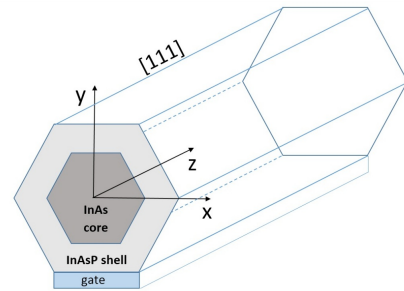


Figure 1. Schematics of a InAs/InAsP CSNW grown along [111] with a bottom gate.

^{a)}Electronic mail: pawel.wojcik@fis.agh.edu.pl

^{b)}Electronic mail: andrea.bertoni@nano.cnr.it

^{c)}Electronic mail: guido.goldoni@unimore.it

allow for an increased flexibility in distorting the electron gas of the NWs, giving rise to a specific, interfacial SOC contribution^{46,47} which substantially increases the total SOC. We make the case for InAs/InAsP CSNWs, a systems of specific interest in photonics⁴⁸ and electrical engineering⁴⁹. Our results qualitatively agree with the recent experiments by Furthmeier *et al.* in Ref. 50, where the enhancement of SO coupling was measured in GaAs/AlGaAs CSNW, and establish a strategy to increase the SOC in Majorana InAs NWs.

We consider CSNWs with hexagonal cross-section⁵¹ grown along [111] (see Fig. 1), assuming in-wire translational invariance along z . The used $\vec{k} \cdot \vec{p}$ approach is described in full in Ref. 5; here we focus on generalizations required to account for the contribution of the internal heterointerface. The 8×8 Kane Hamiltonian is given by¹⁶

$$H_{8 \times 8} = \begin{pmatrix} H_c & H_{cv} \\ H_{cv}^\dagger & H_v \end{pmatrix}, \quad (1)$$

where H_c and H_v are the diagonal matrices corresponding to the conduction (Γ_{6c}) and valence (Γ_{8v} , Γ_{7v}) bands whose expressions are given in Ref. 5. Using the perturbative transformation $\mathcal{H}(E) = H_c + H_{cv}(H_v - E)^{-1}H_{cv}^\dagger$, the Hamiltonian (1) reduces to a 2×2 effective Hamiltonian for the conduction band electrons. Emphasizing the dependence of material parameters on the position, $\vec{p} = (x, y)$,

$$\mathcal{H} = \left[-\frac{\hbar^2}{2} \nabla_{2D} \frac{1}{m^*(\vec{p})} \nabla_{2D} + \frac{\hbar^2 k_z^2}{2m^*(\vec{p})} + E_c(\vec{p}) + V(\vec{p}) \right] \times \mathbf{1}_{2 \times 2} + [\hat{\alpha}_x(\vec{p})\sigma_x + \hat{\alpha}_y(\vec{p})\sigma_y] k_z, \quad (2)$$

where $\sigma_{x(y)}$ are the Pauli matrices and m^* is the effective mass given by

$$\frac{1}{m^*(\vec{p})} = \frac{1}{m_0} + \frac{2P^2}{3\hbar^2} \left(\frac{2}{E_0(\vec{p})} + \frac{1}{E_0(\vec{p}) + \Delta_0(\vec{p})} \right), \quad (3)$$

where P is the conduction-to-valance band coupling parameter.

In Eq. (2), $\hat{\alpha}_x$, $\hat{\alpha}_y$ are the SOC operators

$$\hat{\alpha}_x = \frac{i}{3} P^2 \hat{k}_y \beta(\vec{p}) - \frac{i}{3} P^2 \beta(\vec{p}) \hat{k}_y, \quad (4)$$

$$\hat{\alpha}_y = \frac{i}{3} P^2 \hat{k}_x \beta(\vec{p}) - \frac{i}{3} P^2 \beta(\vec{p}) \hat{k}_x, \quad (5)$$

and $\beta(\vec{p})$ is a material-dependent coefficient obtained as follows. In the i -th layer

$$\beta_i(\vec{p}) = \frac{1}{E_{c,i} + V(\vec{p}) - E_{0,i} - E} - \frac{1}{E_{c,i} + V(\vec{p}) - E_{0,i} - \Delta_{0,i} - E}, \quad (6)$$

where E_c , E_0 and Δ_0 are the conduction band edge, the energy gap and the split-off band gap, respectively. Assuming that the above parameters change as a step-like

function at the interfaces

$$\beta(\vec{p}) = \sum_i [\beta_i(\vec{p}) - \beta_{i+1}(\vec{p})] \Omega_i(\vec{p}), \quad (7)$$

where the sum is carried out over all the layers, and $\Omega_i(\vec{p})$ is the shape function, which for the hexagonal section is given by

$$\Omega_i(\vec{p}) = [\theta(x + x_i) - \theta(x - x_i)][\theta(y + y_i) - \theta(y - y_i)] \times [\theta(x - y + x_i) - \theta(x - y - x_i)], \quad (8)$$

where θ is the Heaviside's function and (x_i, y_i) denotes the position of the (i) -th interface. Further Taylor expansion gives

$$\beta_i(\vec{p}) \approx \left(\frac{1}{E_{0,i} + \Delta_{0,i}} - \frac{1}{E_{0,i}} \right) + \left(\frac{1}{E_{0,i}^2} - \frac{1}{(E_{0,i} + \Delta_{0,i})^2} \right) (E_{c,i} + V(x, y) - E). \quad (9)$$

Substituting (9) into Eqs. (4) and (5), the Rashba coupling constants can be written as

$$\alpha_{x(y)}(\vec{p}) = \alpha_{x(y)}^V(\vec{p}) + \alpha_{x(y)}^{int}(\vec{p}), \quad (10)$$

i.e., the sum of the SOC induced by the electrostatic potential asymmetry,

$$\alpha_{x(y)}^V(\vec{p}) \approx \sum_i \frac{1}{3} P^2 \left(\frac{1}{E_{0,i}^2} - \frac{1}{(E_{0,i} + \Delta_{0,i})^2} \right) \frac{\partial V(\vec{p})}{\partial y(x)}, \quad (11)$$

and the interface SOC, related to the electric field at the interfaces between shells,

$$\alpha_{x(y)}^{int}(\vec{p}) \approx \sum_i \frac{1}{3} P^2 (\tilde{\beta}_i - \tilde{\beta}_{i+1}) \frac{\partial \Omega_i(\vec{p})}{\partial y(x)}, \quad (12)$$

with $\tilde{\beta}_i = \frac{1}{E_{0,i} + \Delta_{0,i}} - \frac{1}{E_{0,i}}$.

Projecting the 3D Hamiltonian (2) on the basis of in-wire states $\psi_n(\vec{p}) \exp(ik_z z)$, where the envelope functions $\psi_n(\vec{p})$ are determined by the strong confinement in the lateral direction, leads to SOC matrix elements

$$\alpha_{x(y)}^{\gamma, nm} = \int \int \psi_n(\vec{p}) \alpha_{x(y)}^\gamma(\vec{p}) \psi_m(\vec{p}) d\vec{p}, \quad (13)$$

where γ identifies the electrostatic ($\gamma = V$) or the interfacial ($\gamma = int$) contribution.

For the NW in Fig. 1 with a single bottom gate, $\alpha_y^{\gamma, nn} = 0$ due to inversion symmetry about y . Moreover, here we focus on the lowest intra-subband coefficient, $n = 1$. Below we discuss the SOC constant $\alpha_R = \alpha_x^{11}$ and corresponding interfacial and electrostatic components, $\alpha_R^\gamma = \alpha_x^{V,11}$ and $\alpha_R^\gamma = \alpha_x^{int,11}$, respectively.

The electronic states in the CSNW section, $\psi_n(\vec{p})$, are calculated by a mean-field self-consistent Schrödinger-Poisson approach⁴⁰. We neglect the exchange-correlation potential which is substantially smaller than the Hartree

	InAs	InAs _{0.9} P _{0.1}
$m^*[m_0]$	0.0265	0.0308
$E_c[\text{eV}]$	0.252	0.3
$E_0[\text{eV}]$	0.42	0.5
$\Delta_0[\text{eV}]$	0.38	0.35

Table I. Bulk parameters used in calculations⁵⁶.

potential^{40,52,53}. The gradient of the self-consistent potential $V(\vec{\rho})$ and the corresponding envelope functions $\psi_n(\vec{\rho})$ are finally used to determine α_R from Eq. (13).

Material parameters mismatch at the interfaces is taken into account solving the eigenproblem $\mathcal{H}\psi_n = E\psi_n$ with boundary conditions^{46,54}

$$\psi_n^{(i)}(\vec{\rho}_k) = \psi_n^{(j)}(\vec{\rho}_k) \quad (14)$$

$$\frac{\hbar^2}{2m^{*(i)}}\nabla_{2D}\psi_n^{(i)}(\vec{\rho}_k) - \frac{\hbar^2}{2m^{*(j)}}\nabla_{2D}\psi_n^{(j)}(\vec{\rho}_k) + [\beta^{(j)}(\vec{\rho}_k) - \beta^{(i)}(\vec{\rho}_k)](\sigma_x + \sigma_y)k_z\psi_n^{(i)}(\vec{\rho}_k) = 0, \quad (15)$$

where $\vec{\rho}_k$ is the position of the interface between i -th and j -th shells. Equations (14), (15), depend on both the potential $V(\vec{\rho})$ at the interface and the energy E . We eliminate this dependence neglecting the term proportional to $(E_{c,i} + V(\vec{\rho}) - E)$ in the Taylor series, Eq. (9). Then, the interface contributions (12) are determined fully by material parameters. This assumption, justified when $\beta^{(j)} - \beta^{(i)}$ is small, neglects the SOC related to the motion of electron in the $\vec{\rho}$ plane, which in general contributes to the SOC by the boundary conditions.

Below we investigate a InAs 50 nm-wide core (measured facet-to-facet) surrounded by a 30 nm InAs_{1-x}P_x shell, with $x = 0.1$ which allows to neglect strain-induced SOC.⁵⁵ Furthermore, as shown below, interfacial SOC is enhanced by the easy penetration of envelope functions in low band offset barriers, here only 48 meV high. Simulations have been carried out for a temperature $T = 4.2$ K, in the constant electron concentration regime. The parameters adopted are given in Tab. I. P is assumed to be constant throughout the materials and $E_P(\text{InAs}) = 2m_0P^2/\hbar^2 = 21.5$ eV.

The calculated SOC coefficients for the InAs/InAsP CSNW of Fig. 1 as a function of the back gate voltage is reported in Fig. 2(a). The SOC constant is trivially zero if $V_g = 0$, due to the overall inversion symmetry. At any finite voltage the inversion symmetry is removed, hence $\alpha_R \neq 0$. As shown in Fig. 2(a), the total α_R ensues from two different contributors, namely interfacial and electrostatic, whose magnitude is of the same order. It is thus crucial to include both of them in the assessment of SOC in CSNWs. Note that the electrostatic component almost coincides with the value for an InAs NW with the same geometry, but no overgrown shell⁵⁷. However, for this specific nanostructure, the largest part of α_R is due to the interfacial contribution, which is $\approx 50\%$ larger than the electrostatic one. While the ratio between the two contributions is nearly independent of V_g [see the in-

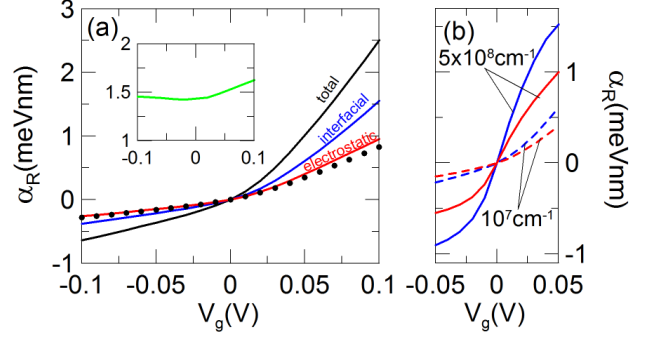


Figure 2. (a) Lines: total, electrostatic and interfacial SOC constants *vs* gate voltage V_g , according to labels. Dots: total SOC constant for an equivalent homogeneous InAs NW. Inset: ratio between interfacial and electrostatic components, $\alpha_R^{int}/\alpha_R^V$. Results for $n_e = 10^7 \text{cm}^{-1}$. See text for structure and material parameters. (b) Electrostatic and interfacial SOC constants *vs* V_g around $V_g = 0$ showing shooting up of SO couplings for higher electron density.

set in Fig. 2(a)], they are both strongly anisotropic with respect to the field direction. This is due to the different effects on the charge density, as discussed in Ref. 5. This effect can also be grasped from the probability distribution reported in Fig. 3 (top and bottom rows). Indeed, the positive V_g pushes electron states towards the interface opposite to the gate, where the gradient of the self-consistent field is low. On the other hand, at $V_g < 0$ electrons are pulled to the region of the nearest interface with the stronger electric field, additionally strengthened by the electron-electron interaction⁵.

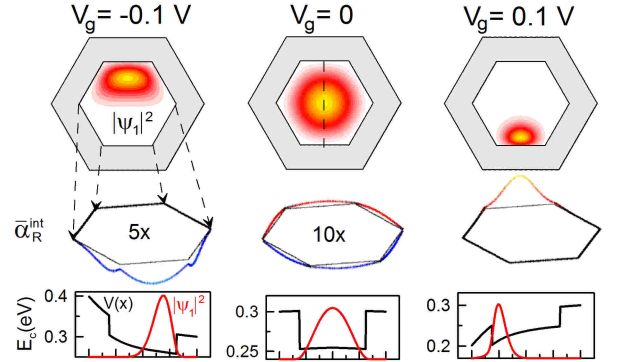


Figure 3. Top row: Square of the ground state envelope function $|\psi_1(x,y)|^2$. Middle row: linear density of the interfacial SOC constants at interfaces. Bottom row: self-consistent potential profile (black line) and $|\psi_1(x,y)|^2$ (red line) along the facet-to-facet dashed line marked in the top-middle panel. Results at selected gate voltages $V_g = -0.1, 0, 0.1$ V for the same structure as in Fig. 2.

The value of α_R^{int} depends on the penetration of the

wave function into the interfaces. As shown in Fig. 3 (middle row) the linear density of interfacial SOC at the interfaces $\bar{\alpha}_R^{int} = \psi_1(\vec{\rho})\alpha_R^{int}(\vec{\rho})\psi_1(\vec{\rho})$ is finite almost everywhere, but it has opposite sign at opposite facets.⁵⁸ For a centro-symmetric system ($V_g = 0$) the overall value is zero, since opposite contributions cancel out exactly. We stress a remarkable difference between CSNWs and analogous planar structures. In a *planar* asymmetric quantum well, for example, $\alpha_R \neq 0$. In a CSNW with an embedded quantum well, however, the overall symmetry is recovered even if each facet of the quantum well is individually asymmetric. Therefore, opposite segments have opposite Rashba contributions and compensate. However, any asymmetric gate potential unbalances opposite contributions, the total effect being related to the amount of envelope function at the interface.

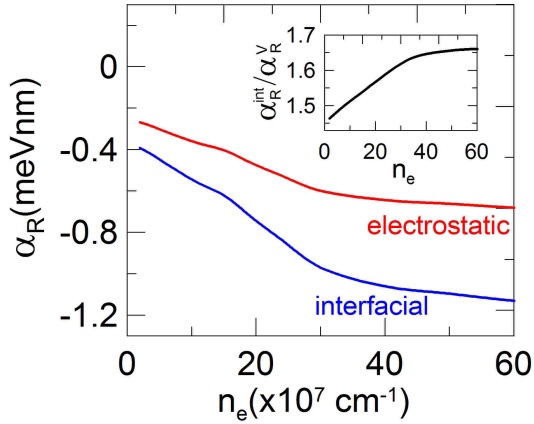


Figure 4. Electrostatic α_R^V and interfacial α_R^{int} contributions of SOC constant *vs* electron density n_e . Results for $V_g = -0.1$ V. Inset: ratio $\alpha_R^{int}/\alpha_R^V$ *vs* n_e .

Note the almost linear increase of α_R with V_g . This behaviour is observed in a relatively small charge density regime: the average Coulomb energy is small, most of the charge is located in the core, and it is relatively rigid to an applied transverse electric field. At larger densities, however, charge moves at the interfaces to minimize Coulomb interaction⁴⁰, with negligible tunneling energy between opposite facets. In this regime, the symmetric charge density distribution is unstable and it is easily distorted by an electric field⁵. Accordingly, SOC constant shoots around $V_g = 0$ as soon as the gate is switched on - see Fig. 2(b).

As we show in Fig. 4, both SOC components substantially increase in intensity with charge density, while their ratio is weakly affected, it being rather a *property of the nano-material* (band parameters and band offset). This is explicitly shown in Fig. 5, where the two contributions are plot *vs* the stoichiometric fraction x . At low x , penetration is very large, and the interfacial effect is dominant (of course for $x = 0$ the heterostructure is an homogeneous NW with a larger diameter), while as $x = 0.15$ the two contributions are comparable, as also shown in the

inset.

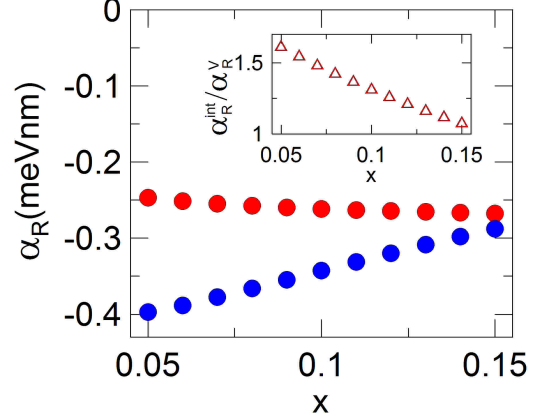


Figure 5. The interfacial α_R^{int} (blue circles) and electrostatic α_R^V (red circles) SOC constants *vs* InAs_{1-x}P_x alloy composition, x . Inset: $\alpha_R^{int}/\alpha_R^V$ *vs* x . Results for $V_g = -0.1$ V and $n_e = 10^7$ cm⁻².

To summarize, we have shown that Rashba SOC in CSNWs is increased by the effect of the radial heterointerface, and its control via external metallic gates may be highly improved by this interfacial effect. Although we did not attempt to optimize α_R in the many parameter space allowed by CSNWs, our results suggest that a general strategy to enhance SOC in CSNWs relies on a modification of the compositional structure exploiting asymmetric penetration of the wave function into the shell layer.

This work was partially supported by the AGH UST statutory tasks No. 11.11.220.01/2 within subsidy of the Ministry of Science and Higher Education and in part by PL-Grid Infrastructure. P.W. was supported by National Science Centre, Poland (NCN) according to decision 2017/26/D/ST3/00109.

REFERENCES

- ¹I. A. Kokurin, Physica E **74**, 264 (2015).
- ²I. A. Kokurin, Solid State. Commun. **195**, 49 (2014).
- ³M. Kammermeier, P. Wenk, J. Schliemann, S. Heedt, and T. Schäpers, Phys. Rev. B **93**, 205306 (2016).
- ⁴G. W. Winkler, D. Varjas, R. Skolasinski, A. A. Soluyanov, M. Troyer, and M. Wimmer, Phys. Rev. Lett. **119**, 037701 (2017).
- ⁵P. Wójcik, A. Bertoni, and G. Goldoni, Phys. Rev. B **97**, 165401 (2018).
- ⁶T. Campos, P. E. Faria Junior, M. Gmitra, G. M. Sipahi, and J. Fabian, Phys. Rev. B **97**, 245402 (2018).
- ⁷J.-W. Luo, S.-S. Li, and A. Zunger, Phys. Rev. Lett. **119**, 126401 (2017).
- ⁸J. Alicea, Phys. Rev. B **81**, 125318 (2010).
- ⁹J. Sau, Physics **10**, 68 (2017).
- ¹⁰A. Kitaev, Ann. Phys. **303**, 2 (2003).
- ¹¹J. D. Sau, S. Tewari, and S. Das Sarma, Phys. Rev. B **85**, 1 (2012).

- ¹²V. Mourik, K. Zuo, S. M. Frolov, S. R. Plissard, E. P. A. M. Bakkers, and L. P. Kouwenhoven, *Science* **336**, 1003 (2012).
- ¹³J. Mastomäki, S. Roddaro, M. Rocci, V. Zannier, D. Ercolani, L. Sorba, I. J. Maasilta, N. Ligato, A. Fornieri, E. Strambini, and F. Giazotto, *Nano Research* **10**, 3468 (2017).
- ¹⁴S. M. Albrecht, A. P. Higginbotham, M. Madsen, F. Kuemmeth, T. S. Jespersen, J. Nygård, P. Krogstrup, and C. M. Marcus, *Nature* **531**, 206 (2016).
- ¹⁵A. Manolescu, A. Sitek, J. Osca, L. m. c. Serra, V. Gudmundsson, and T. D. Stanescu, *Phys. Rev. B* **96**, 125435 (2017).
- ¹⁶J. Fabian, A. Matos-Abiad, C. Ertler, P. Stano, and I. Žutić, *Acta Physica Slovaca* **57**, 565 (2007).
- ¹⁷S. Datta and B. Das, *Appl. Phys. Lett.* **56**, 665 (1990).
- ¹⁸J. Schliemann, J. C. Egues, and D. Loss, *Phys. Rev. Lett.* **90**, 146801 (2003).
- ¹⁹P. Wójcik and J. Adamowski, *Semicond. Sci. Technol.* **31**, 115012 (2016).
- ²⁰P. Wójcik, J. Adamowski, B. J. Spisak, and M. Wołoszyn, *J. Appl. Phys.* **115**, 104310 (2014).
- ²¹P. Wójcik and J. Adamowski, *Sci Rep* **7**, 45346 (2017).
- ²²P. P. Das, J. Bhandari, N. abd Wan, M. Cahay, K. B. Chetry, R. S. Newrock, and S. T. Herbert, *Nanotechnology* **23**, 215201 (2012).
- ²³P. Debray, S. Rahman, and M. Muhammad, *Nature Nano Technol.* **4**, 759 (2009).
- ²⁴M. Kohda, S. Nakamura, Y. Nishihara, K. Kobayashi, T. Ono, J. O. Ohe, Y. Tokura, T. Mineno, and J. Nitta, *Nature Communications* **3**, 1082 (2012).
- ²⁵F. Rossella, A. Bertoni, D. Ercolani, M. Rontani, L. Sorba, F. Beltram, and S. Roddaro, *Nat. Nanotechnol.* **9**, 997 (2014).
- ²⁶A. Iorio, M. Rocci, L. Bours, M. Carrega, V. Zannier, L. Sorba, S. Roddaro, F. Giazotto, and E. Strambini, *ArXiv e-prints* (2018), arXiv:1807.04344 [cond-mat.mes-hall].
- ²⁷E. I. Rashba, *Sov. Phys. Solid State* **2**, 1109 (1960).
- ²⁸G. Dresselhaus, *Phys. Rev.* **100**, 580 (1955).
- ²⁹I. van Weperen, B. Tarasinski, D. Eeltink, V. S. Pribyl, S. R. Plissard, E. P. A. M. Bakkers, L. P. Kouwenhoven, and M. Wimmer, *Phys. Rev. B* **91**, 201413(R) (2015).
- ³⁰J. Kammhuber, M. C. Cassidy, F. Pei, M. P. Nowak, A. Vuik, D. Car, S. R. Plissard, E. P. A. M. Bakkers, M. Wimmer, and L. P. Kouwenhoven, *Nat Commun.* **8**, 478 (2017).
- ³¹Z. Scherübl, G. m. H. Fülöp, M. H. Madsen, J. Nygård, and S. Csonka, *Phys. Rev. B* **94**, 035444 (2016).
- ³²A. E. Hansen, M. T. Björk, C. Fasth, C. Thelander, and L. Samuelson, *Phys. Rev. B* **71**, 205328 (2005).
- ³³S. Dhara, H. S. Solanki, V. Singh, A. Narayanan, P. Chaudhari, M. Gokhale, A. Bhattacharya, and M. M. Deshmukh, *Phys. Rev. B* **79**, 121311 (2009).
- ³⁴P. Roulleau, T. Choi, S. Riedi, T. Heinzl, I. Shorubalko, T. Ihn, and K. Ensslin, *Phys. Rev. B* **81**, 155449 (2010).
- ³⁵S. Estévez Hernández, M. Akabori, K. Sladek, C. Volk, S. Alagha, H. Hardtdegen, M. G. Pala, N. Demarina, D. Grützmacher, and T. Schäpers, *Phys. Rev. B* **82**, 235303 (2010).
- ³⁶P. Wójcik, A. Bertoni, and G. Goldoni, (2018), unpublished.
- ³⁷R. L. Kallaher, J. J. Heremans, N. Goel, S. J. Chung, and M. B. Santos, *Phys. Rev. B* **81**, 0035335 (2010).
- ³⁸R. L. Kallaher, J. J. Heremans, N. Goel, S. J. Chung, and M. B. Santos, *Phys. Rev. B* **81**, 075303 (2010).
- ³⁹F. Herling, C. Morrison, C. S. Knox, S. Zhang, O. Newell, M. Myronov, E. H. Linfield, and C. H. Marrows, *Phys. Rev. B* **95**, 155307 (2017).
- ⁴⁰A. Bertoni, M. Royo, F. Mahawish, and G. Goldoni, *Phys. Rev. B* **84**, 205323 (2011).
- ⁴¹S. Funk, M. Royo, I. Zardo, D. Rudolph, S. Morktter, B. Mayer, J. Becker, A. Bechtold, S. Matich, M. Dblinger, M. Bichler, G. Koblmüller, J. J. Finley, A. Bertoni, G. Goldoni, and G. Abstreiter, *Nano Letters* **13**, 6189 (2013).
- ⁴²J. Jadcak, P. Plochocka, A. Mitioglu, I. Breslavetz, M. Royo, A. Bertoni, G. Goldoni, T. Smolenski, P. Kossacki, A. Kretinin, H. Shtrikman, and D. K. Maude, *Nano Letters* **14**, 2807 (2014).
- ⁴³M. Royo, A. Bertoni, and G. Goldoni, *Phys. Rev. B* **89**, 155416 (2014).
- ⁴⁴F. Jabeen, S. Rubini, V. Grillo, L. Felisari, and F. Martelli, *Appl. Phys. Lett.* **93**, 083117 (2008).
- ⁴⁵D. Spirkoska, J. Arbiol, A. Gustafsson, S. Conesa-Boj, F. Glas, I. Zardo, M. Heigoldt, M. H. Gass, A. L. Bleloch, S. Estrade, M. Kaniber, J. Rossler, F. Peiro, J. R. Morante, G. Abstreiter, L. Samuelson, and A. Fontcuberta i Morral, *Phys. Rev. B* **80**, 245325 (2009).
- ⁴⁶Z. A. Devizorova and V. A. Volkov, *JETP Lett.* **98**, 101 (2013).
- ⁴⁷E. L. Ivchenko, A. Y. Kaminski, and U. Rössler, *Phys. Rev. B* **54**, 5852 (1996).
- ⁴⁸J. Treu, M. Bormann, H. Schmeiduch, M. Dblinger, S. Morktter, S. Matich, P. Wiecha, K. Saller, B. Mayer, M. Bichler, M.-C. Amann, J. J. Finley, G. Abstreiter, and G. Koblmüller, *Nano Letters* **13**, 6070 (2013).
- ⁴⁹X. Liu, P. Liu, H. Huang, C. Chen, T. Jin, Y. Zhang, X. Huang, Z. Jin, X. Li, and Z. Tang, *Nanotechnology* **24**, 245306 (2013).
- ⁵⁰S. Furthmeier, F. Dirnberger, M. Gmitra, A. Bayer, M. Forsch, J. Hubmann, C. Schüller, E. Reiger, J. Fabian, T. Korn, and D. Bougeard, *Nat Commun.* **7**, 12413 (2016).
- ⁵¹A. Sitek, M. Urbaneja Torres, K. Torfason, V. Gudmundsson, A. Bertoni, and A. Manolescu, *Nano Letters* **18**, 2581 (2018).
- ⁵²B. M. Wong, F. Lonard, Q. Li, and G. T. Wang, *Nano Letters* **11**, 3074 (2011).
- ⁵³M. Royo, C. Segarra, A. Bertoni, G. Goldoni, and J. Planelles, *Phys. Rev. B* **91**, 115440 (2015).
- ⁵⁴E. A. de Andrada e Silva, G. C. La Rocca, and F. Bassani, *Phys. Rev. B* **55**, 16293 (1997).
- ⁵⁵Lattice mismatch and strain field are additional sources of SOC, which are neglected for the present lattice matched heterostructures. We also neglect a SOC contribution resulting from the interface inversion asymmetry related to different atomic termination at opposite interfaces^{59,60} which is small. Moreover, additional calculations with slight smearing of the potential at the interface instead of the step like function did not lead to significantly different results.
- ⁵⁶I. Vurgaftman, J. R. Meyer, and L. R. Ram-Mohan, *J. Appl. Phys.* **89**, 5815 (2001).
- ⁵⁷For the model CSNW under consideration, the gate is attached directly to the NW, so that α_R is an upper bound value, while any dielectric interlayer would decrease α_R . For the NW with no shell, the gate has been placed at the same distance from the core as in the case with the shell, in order to compare the two calculations.
- ⁵⁸The sign of the SOC linear density on each facet is decided by the choice of the reference frame. Since $\hat{\alpha}_x$ appears combined with the spin matrices in the Hamiltonian (2), the overall sign of the SOC term is unaffected by a change in the reference frame.
- ⁵⁹E. L. Ivchenko, A. Y. Kaminski, and U. Rössler, *Phys. Rev. B* **54**, 5852 (1996).
- ⁶⁰U. Rössler and J. Kainz, *Solid State Commun.* **121**, 313 (2002).